ARTICLES
https://doi.org/10.1038/s41557-021-00824-w

nature chemistry

Bottom-up fabrication of a proteasome–nanopore that unravels and processes single proteins

Shengli Zhang, Gang Huang, Roderick Corstiaan Abraham Versloot, Bart Marlon Herwig Bruininks, Paulo Cesar Telles de Souza, Siewert-Jan Marrink and Giovanni Maglia ✉

The precise assembly and engineering of molecular machines capable of handling biomolecules play crucial roles in most single-molecule methods. In this work we use components from all three domains of life to fabricate an integrated multiprotein complex that controls the unfolding and threading of individual proteins across a nanopore. This 900 kDa multicomponent device was made in two steps. First, we designed a stable and low-noise β-barrel nanopore sensor by linking the transmembrane region of bacterial protective antigen to a mammalian proteasome activator. An archaeal 20S proteasome was then built into the artificial nanopore to control the unfolding and linearized transport of proteins across the nanopore. This multicomponent molecular machine opens the door to two approaches in single-molecule protein analysis, in which selected substrate proteins are unfolded, fed to into the proteasomal chamber and then addressed either as fragmented peptides or intact polypeptides.

Membrane-spanning channels and pores have key roles in cellular processes and in biotechnological applications such as nanopore DNA sequencing[1]. A nanopore protein sequencing device requires the unravelling of a protein and the recognition of individual amino acids by ionic currents as the polypeptide is transported across the nanopore. Several studies revealed that tiny differences between molecules can be identified by nanopore currents[2–7], suggesting that amino acid recognition should be a tractable problem. One of the main remaining challenges is to design a nanopore sensor capable of unfolding proteins without influencing the ionic signal[8,9]. Small transmembrane proteins have been designed to control the passive transport of ions across membranes, including a synthetic ion channel[10], a four-helix divalent metal-ion transporter[11], membrane-spanning pores[12,13] and a DNA-scaffolded pore[14]; however, the ability to design nanopores with an integrated biopolymer handling unit has not been done. Such devices would add a new dimension to the protein engineering field and allow designing next-generation nanopore sensors for biopolymer analysis. Advances in this field have nonetheless been hampered for a number of reasons. Usually, molecular machines form multimeric complexes that require complex post- and co-translational assembly[15]. The latter is particularly challenging as all components must be soluble, unprocessed by proteases and co-expressed at similar levels. The introduction of artificial transmembrane regions provides an extra challenge as it reduces the solubility of the individual component and it can prevent proper assembly. Moreover, the design of the interface between the hydrophobic transmembrane polypeptides and the hydrophilic components remains unexplored. Finally, to obtain a functional device, the nanopore should remain constantly open and the operation of the molecular machine should not occlude the nanopore sensor.

In this work we addressed all of these challenges and fabricated in two steps a 42-component 900 kDa integrated nanopore sensor that consists of three co-assembled proteins. In the first step, aided by molecular dynamic simulations, we devise a strategy to design artificial nanopores from a soluble protein with a toroid shape (Fig. 1a–d). The designed synthetic nanopores exhibited activities and electrical properties identical to the nanopores found in nature. In the second step, the multiprotein 20S proteasome from *Thermoplasma acidophilum*[16] was incorporated into the artificial nanopore (Fig. 1e–h). This design allows two approaches to single-molecule protein analysis including sequencing. In the chop-and-drop mode, unfolded proteins are first degraded by the proteasome and the resulting fragment delivered to the nanopore. In the thread-and-read mode, intact substrates are detected as they translocate across the nanopore. Notably, the activity of the proteasome and the unfolding of proteins did not have an influence on the ionic signal.

Results and discussion

Design of transmembrane proteins. In cells, heptameric proteasome activator 28α regulates the function of the proteasome by docking on the heptameric 20S core proteasome particle[17]. Hence, in the first step to build a proteasome–nanopore, we designed a nanopore based on the proteasome activator 28α (also called REG or 11S activators[18], *Mus musculus*; Figs. 1a and 2a). The disorder region of REG (from P64 to P100) was replaced with the β-barrel transmembrane region (VHGNAEVHASFFDIGGSVSAGF) of the heptameric anthrax protective antigen nanopore[19] (*Bacillus anthracis*; Fig. 2a and Supplementary Fig. 1). A β-barrel transmembrane region was chosen because it offers high thermodynamic stability and can tolerate many sequences substitutions[20,21]. A short flexible and hydrophilic linker (SSG) was added to each side of the β-barrel (Fig. 1a–d, Fig. 2a and Supplementary Fig. 1) to mediate the interaction between the transmembrane part of anthrax protective antigen and REG, and to provide a passage for the ion to enter the nanopore.

Despite that the 22 residues of this transmembrane region are sufficient to span the hydrophobic core of a lipid bilayer, the initial construct did not insert into a lipid bilayer (Fig. 2b). As the length of the linker is likely to play an essential role in guiding membrane insertion and controlling the transmembrane ionic transport, we tested one deletion mutant (Δ2) and five insertion mutants (∇2, ∇4, ∇8, ∇12 and ∇16; Fig. 2b). With the exception of Δ2, all variants could insert into the lipid bilayer, although with different efficiencies. Mutants ∇8, ∇12 and ∇16 showed large current fluctuations, which prevented nanopore characterization (Supplementary Fig. 2).

Groningen Biomolecular Sciences and Biotechnology Institute, University of Groningen, Groningen, the Netherlands. ✉e-mail: g.maglia@rug.nl

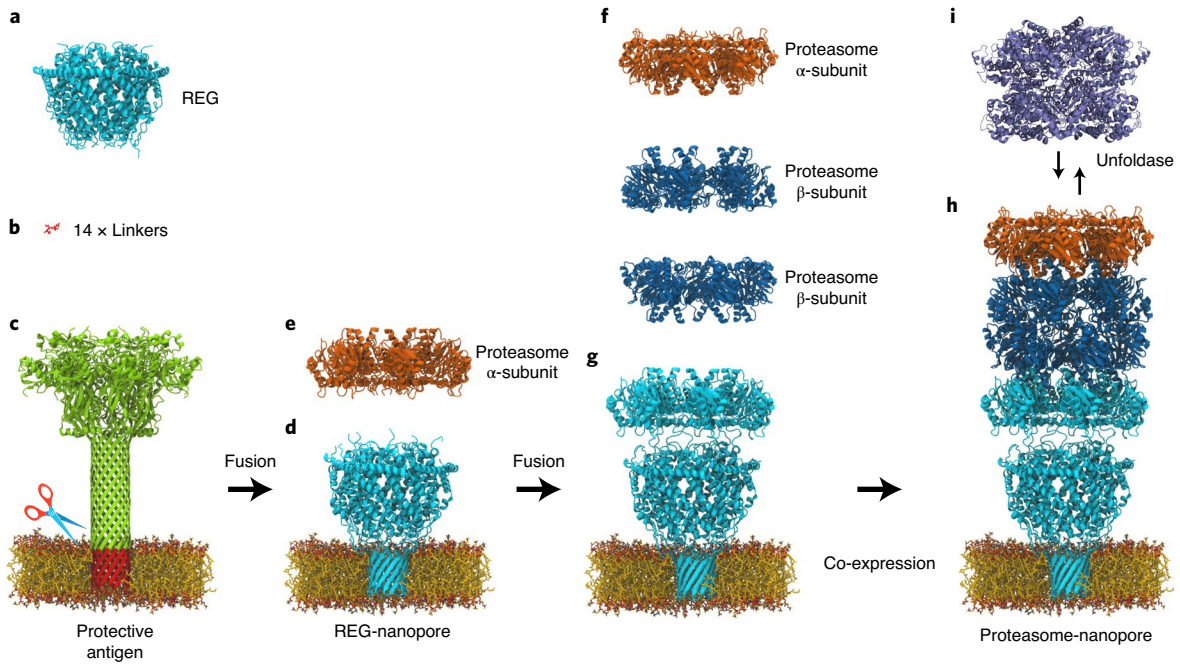

Fig. 1 | Design of a proteasome–nanopore. a, Structure of mouse REG (PDB ID: 5MSJ). **b**, A sticks diagram of the structure of serine–serine–glycine linker. **c**, A ribbon diagram of the structure of anthrax protective antigen (PDB ID: 3J9C). The transmembrane region of the protective antigen is in red. **d**, The structure of the REG–nanopore enhanced by molecular dynamics simulations. REG (**a**) was genetically fused to the transmembrane region of the protective antigen (**c**) via a short linker (**b**). **e**,**f**, The structure of the *T. acidophilum* proteasome α-and β-subunits (PDB ID: 1YA7). **g**, The REG–nanopore was genetically fused to α-subunit of *T. acidophilum* proteasome. **h**, The structure of the designed proteasome–nanopore refined by molecular dynamics simulations. **i**, The structure of VATΔN (PDB ID: 5G4G).

The ∇4 mutant showed full current blocks and a heterogeneous unitary conductance (Fig. 2c). Among all constructs tested, ∇2, which was efficiently expressed and purified (Supplementary Fig. 3), produced uniform pores in lipid bilayers with mean unitary conductance (1.17 ± 0.14 nS at −35 mV, 1 M NaCl, 15 mM Tris, pH 7.5, $n = 59$; Fig. 2d). Remarkably, ∇2-REG-PA-nanopore (hereafter reffered to as a REG–nanopore) inserted as efficiently and uniformly as other nanopores found in nature (for example, alpha-hemolysin[22]) and remained open indefinitely in the lipid bilayer (Supplementary Fig. 4a). The individual peptides corresponding to the transmembrane region of anthrax protective antigen could not form nanopores, indicating that a soluble scaffold is required to stabilize the nanopore in lipid bilayers. Transmission electron microscopy (TEM) images showed that the REG-nanopores assemble into oligomers (Supplementary Fig. 5a).

We first generalized the linker sequence to validate this design principle. We found that amino acid substitutions with serine residues were well tolerated (Fig. 2e). Hence, the β-barrel sequence elongated by linkers containing five serine residues was introduced in two additional soluble proteins. The first was a AAA + ATPase domain of *Aquifex aeolicus*, which activates the transcription σ54-RNA polymerase[23] (Fig. 2f and Supplementary Fig. 1). The second was PA26, a proteasome activator from *Trypanosoma brucei*[18] (Fig. 2g and Supplementary Fig. 1). Both proteins inserted into lipid bilayers and formed open nanopores despite having different diameters and surface residues, indicating that the β-barrel transmembrane domain and a five-amino acid hydrophilic linker allows a generic method to introduce soluble proteins into lipid bilayers for biopolymer analysis. REG was preferred to PA26 as the latter occasionally closed in planar lipid bilayers (Fig. 2g).

Functional properties of the optimized artificial nanopore. Molecular dynamics simulations were performed on the REG–nanopore construct to better understand the electrostatic and hydrophobic interactions between the nanopore and the lipid bilayer. As shown in Figs. 2a and 3a, two rings of hydrophobic residues anchor the transmembrane region to the hydrophobic edges of the bilayer, while alternated residues with aliphatic side-chains interface the core of the bilayer. The lumen of the pore is kept hydrated by hydrophilic residues. As expected, the hydrophilic side-chain of the linker residues are interacting with the charged head groups of membrane lipids. Inside the β-barrel region, the REG–nanopore showed an increased occupancy of cations compared with anions (Supplementary Fig. 6). Similar to other β-barrel nanopores such as αHL[22], REG-nanopores showed an asymmetric current–voltage (I–V) relationship (Fig. 3b,c). Ion selectivity measurements using asymmetric NaCl concentrations (0.5 M/*trans* and 2.0 M/*cis*) confirmed that the nanopore is cation selective (permeability ratio $(P_{Na^+}/P_{Cl^-}) = 1.90 \pm 0.18$; Fig. 3d). Here and throughout the manuscript, uncertainties indicate the standard deviations obtained from at least three experiments. The correct folding of the REG–nanopore in the lipid bilayer was characterized using cyclodextrins (CDs)—circular molecules that bind to β-barrel nanopores[24]. α-CD, β-CD and γ-CD were added to the *cis* side of the artificial nanopore and the magnitude of the ionic current associated with a blockade (I_B) was measured. It was reported that only β-CD and γ-CD can block anthrax protective antigen nanopores[25], presumably because α-CD translocates too quickly to be observed. Accordingly, α-CD blockades were not observed (Supplementary Fig. 7a). β-CD induced fast blockades (spikes), which most likely reflects fast transport across the nanopore (Fig. 3e). γ-CD exhibited characteristic blockades (Fig. 3f). Recordings with the αHL nanopore showed that imipramine induce more blockades when added to the solution[24], reflecting the binding of the analyte to cyclodextrin molecules inside the nanopore. Accordingly, REG-nanopores also induced further analyte blockades in the presence of γ-CD (Fig. 3g),

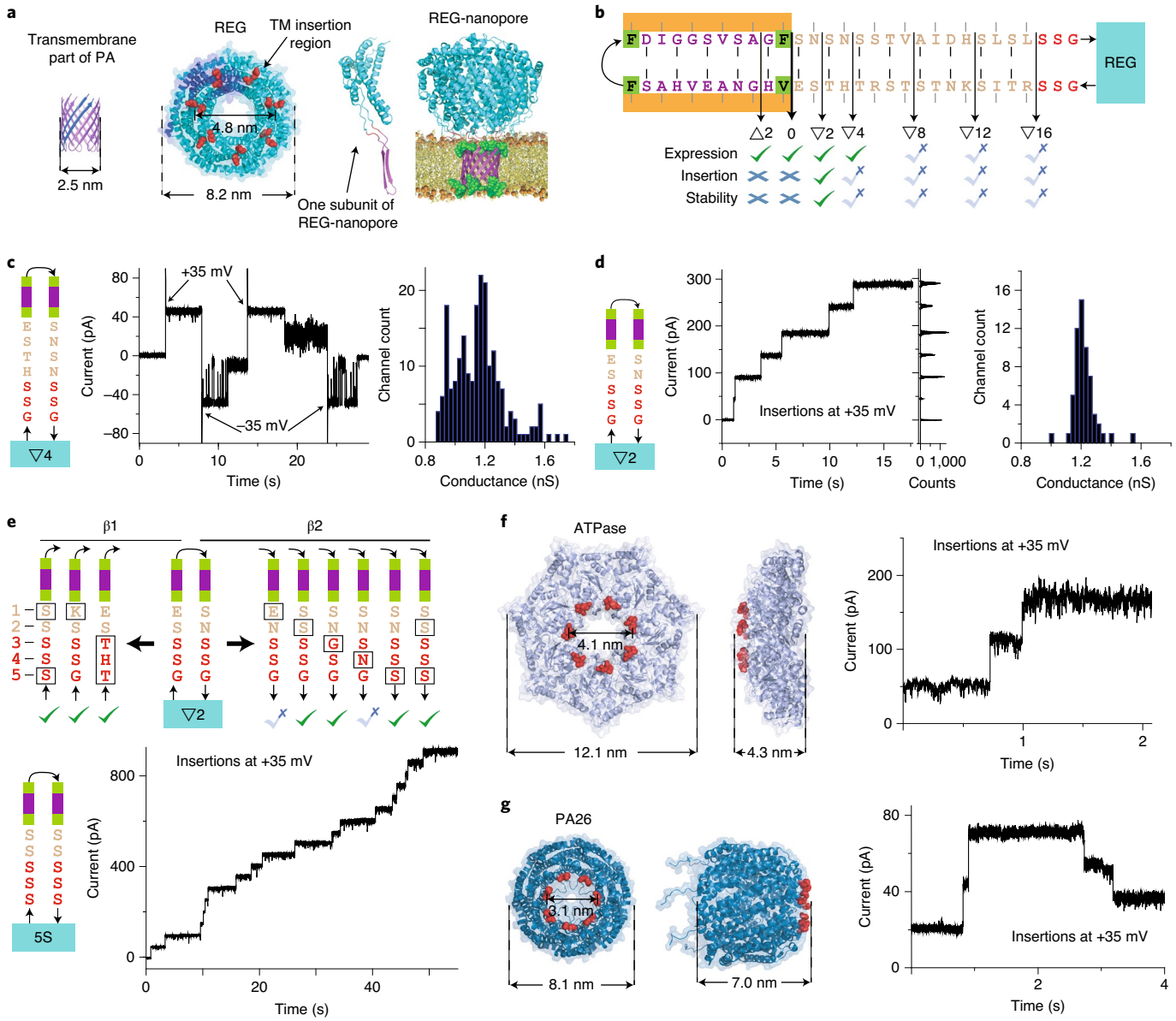

Fig. 2 | Fabrication and optimization of the artificial nanopores. a, A structural representation of the designed REG-nanopore. The heptameric transmembrane part of the protective antigen (PA) replaced an unstructured loop (red) in REG (cyan). One subunit in the transmembrane region and REG is highlighted in blue and showed in isolation. The hydrophobic residues anchoring the nanopore to the membrane are indicated in green. The REG-nanopore was generated by molecular dynamics simulations. **b**, Effects of linker length on the nanopore expression in *E. coli*. cells, insertion efficiency and nanopore stability. The side-chains that point towards the outside and inside of the barrel are highlighted by grey and black lines, respectively. The first designed nanopore (0) is highlighted with a wider arrow. The sequence of the protective antigen was used as template for the linker. REG is shown as a cyan rectangle. **c**,**d**, Electrical properties of the functional ∇4 (**c**) and ∇2 (**d**) mutants. On the left is the sequence of the mutant, in the middle a typical current trace, and on the right the current histogram corresponding the insertions of multiple pores at +35 mV. **e**, Top: linker optimization tested by substituting several residues. Bottom: electrical properties of the REG-nanopore with homopolymeric serine linkers. **f**, The ATPase-nanopore formed by introducing the transmembrane barrel elongated by the homopolymeric serine linkers into a loop (red) at the AAA+ ATPase domain of *Trypanosoma brucei* σ54-RNA polymerase. **g**, The PA26-nanopore formed by introducing the β-barrel elongated by the serine linker into a loop in the top face of PA26 from *Aquifex aeolicus*. Electrical data were collected at ±35 mV in 1 M NaCl, 15 mM Tris, pH 7.5, using 10 kHz sampling rate and a 2 kHz low-pass Bessel filter.

and reduced average spike current values of the blockades induced by β-CD (Supplementary Fig. 7b–d), indicating a binding between the CD adaptors and the analyte. Finally, the ability of the nanopore to identify peptides was tested using angiotensin I (ten amino acids, with a net charge of zero) and dynorphin A (17 amino acids, with a net charge of +4). We found that the two peptides induced blockades, which could be distinguished in mixture using several parameters, including the residual current and the duration of the current blockades (Fig. 3h–j). Peptides smaller than angiotensin II (eight amino acids, with a net charge of zero) could not be observed by nanopore recordings (Supplementary Fig. 7e), thus providing an approximative detection limit of oligopeptide detection using the REG–nanopore.

Building a proteasome–nanopore. In the second and final step, the REG–nanopore is fused with the 20S proteasome from *T. acidophilum*.

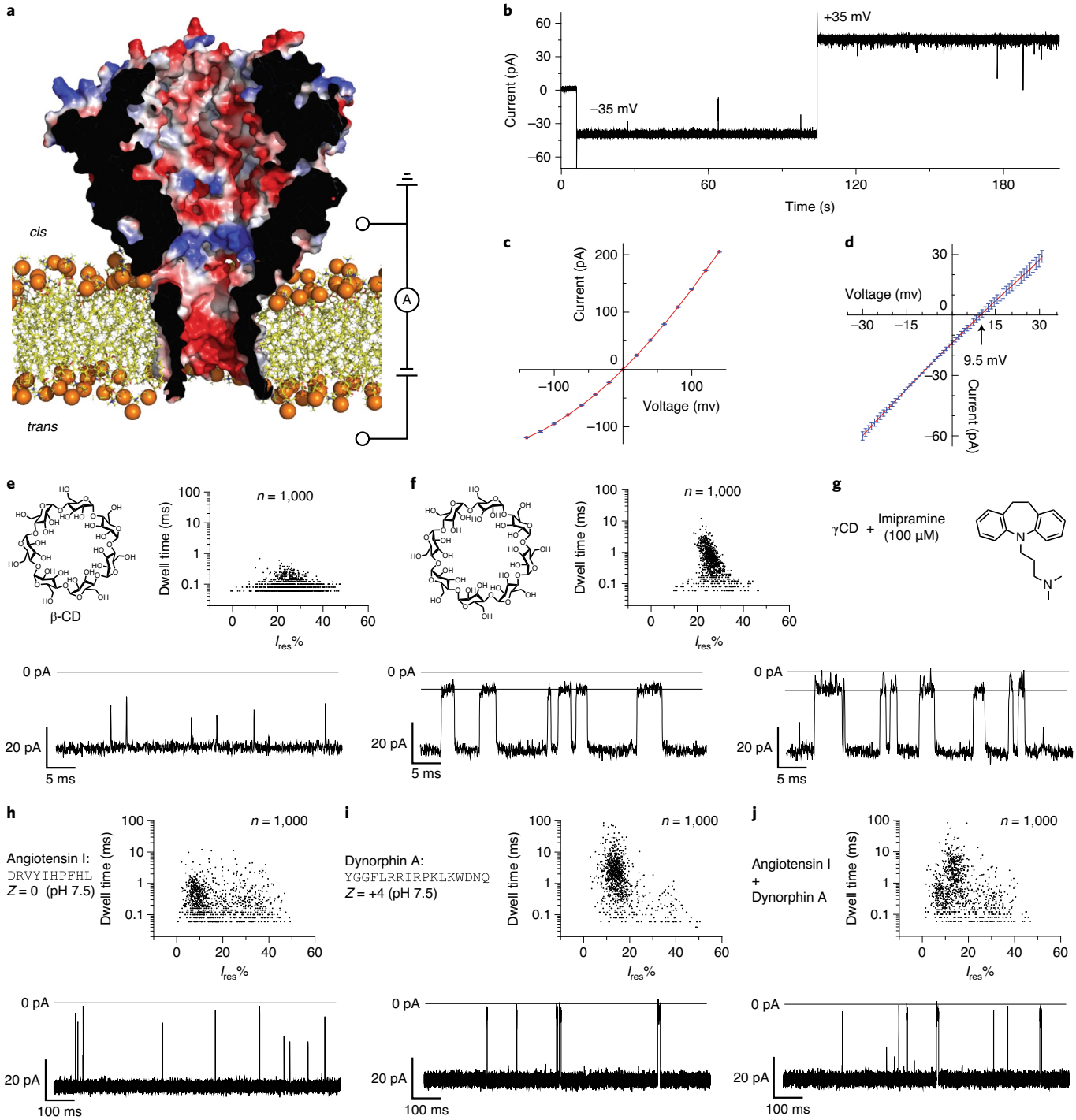

Fig. 3 | Electrical properties of the REG-nanopore. a, Cut-through of a surface representation of the REG-nanopore. The pore is coloured according to the vacuum electrostatic potential as calculated by PyMOL on the final snapshot of the multiscale molecular dynamics model. **b**, A typical current trace recorded of a single REG-nanopore at +35 mV and −35 mV. **c**, Current–voltage characteristics of three different nanopores. **d**, Reversal potential measured using asymmetric ion concentrations (*trans*:*cis*, 0.5 M NaCl: 2.0 M NaCl), showing that the pore is cation selective, as expected from the electrostatic potentials of the nanopore lumen. The REG-nanopore was added to the *trans* side. **e**,**f**, Chemical structures of β-CD (**e**) and γ-CD (**f**) (top left), scatter plots of I_{res}% versus dwell time (top right), and representative traces of 20 μM β-CD (**e**) and γ-CD (**f**) blockades (below). **g**, Chemical structure of imipramine and a representative trace of γ-CD blockades (20 μM) in the presence of 100 μM of imipramine. **h**–**j**, Typical peptide blockades (bottom) and the resulting scatter plots of I_{res}% versus dwell time (top) for 4 μM of angiotensin I (**h**), 4 μM dynorphin A (**i**) and a 2 μM equimolar mixture of the two (**j**). The REG-nanopore and all analytes were added to the *cis* side. Electrical recordings were collected at −35 mV in 1 M NaCl, 15 mM Tris, pH 7.5. All traces except those in **b** were sampled at 50 kHz sampling rate and a 10 kHz low-pass Bessel filter, and an additional Gaussian low-pass filter with a 5 kHz cut-off was digitally applied. In **b**, data were collected at 10 kHz sampling rate and a 2 kHz low-pass Bessel filter.

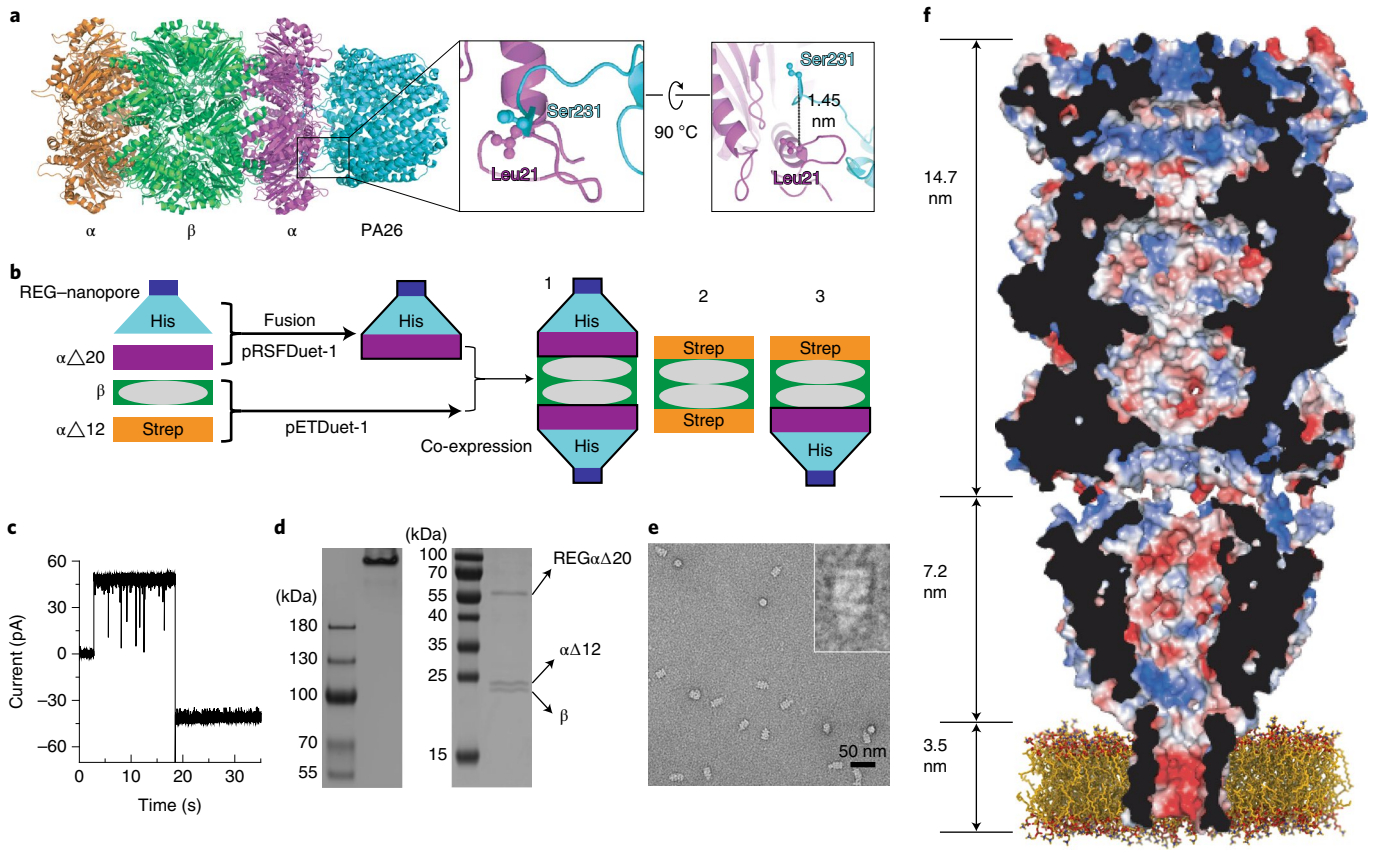

Fig. 4 | Design of the artificial proteasome–nanopore. a, The structure of the *T. acidophilum* proteasome (the α-subunit is orange and magenta, whereas the β-subunit is green) in complex with PA26 (cyan). The C-terminal of PA26 (S231) is near L21 of the proteasome α-subunit. **b**, A representation of the reconstitution of the artificial proteasomal nanopore. To obtain complex **3**, two separate vectors were used to express the three proteins. The REG–nanopore was fused to the proteasome α-subunit and contained a His-tag. The protein was co-expressed with the untagged β-subunits and a second α-subunit containing a Strep-tag. His-tag affinity chromatography was used to co-purify complex **1** and **3**. A Strep-Tag affinity chromatography was then used to purify **3**. **c**, Electrical behaviour of a single pore at ±35 mV in 1 M NaCl, 15 mM Tris, pH 7.5, using 10 kHz sampling rate and a 2 kHz low-pass Bessel filter. **d**, Native PAGE (left, ~5 μg) and SDS-PAGE (right, ~2 μg) analyses of the purified complex **3**. SDS-PAGE revealed the presence of three unique bands corresponding well the molecular weights of REGαΔ20, proteasome α△12-subunit, and proteasome β-subunit (51.8, 25.9 and 22.3 kDa). The native PAGE showed that REGαΔ20, proteasome αΔ12-subunit, and proteasome β-subunit form a stable complex **3**. **e**, A TEM image of the proteasome–nanopore. **f**, Cut-through of a surface representation of proteasome–nanopore enhanced by molecular dynamics simulations and coloured (blue, positive; red, negative) according to the vacuum electrostatic potential as calculated by PyMOL.

The latter is made by four stacked rings composed of 14 α- and 14 β-subunits (Fig. 1e,f)[16]. The two-flanking outer α-rings allow for the association of the 20S proteasome with several regulatory complexes[26], among which is proteasome activator REG (Fig. 1a)[27]; however, we found that no clear interaction was observed when the proteasome was added to the *cis* side of an individual REG–nanopore. This is probably as the high ionic strength used (1 M NaCl) does not permit such an interaction[28]. The crystal structure of the *T. acidophilum* proteasome in complex with PA26 from *Trypanosoma brucei*[18]—a homologue of REG—shows that the carboxy-terminal tails of PA26 slide into a pocket on the 20S proteasome, near the amino-terminus of the α-subunit (Fig. 4a). Hence, we fused the C-terminal of REG (Y249 in REG corresponding to S231 in PA26; Fig. 4a) with L21 of a proteasome α-subunit, in which the first 20 residues are removed (Δ20-α-subunit), leaving the proteasome gate open towards the REG–nanopore. The formation of the proteasome requires co-assembly of the α and β-subunits; thus, (1) a REG–nanopore fused to a proteasome Δ20-α-subunit (REGα△20 nanopore) containing a C-terminal His-tag, (2) a second opened proteasomal subunit (αΔ12, where the first 12 residues are removed allowing the fast degradation of unfolded substrates without the need for a proteasome activator[29]) containing a C-terminal Strep-tag and (3) the proteasome β-subunit were co-expressed in *Escherichia coli* (*E. coli*) cells using a two-vector system (Supplementary Methods and Fig. 4b). Although all proteins could be expressed, sodium dodecyl sulphate–polyacrylamide gel electrophoresis (SDS-PAGE) analysis indicated that the proteasome–nanopore was proteolytically cleaved inside *E. coli* cells during expression (Supplementary Fig. 8b). Proteolysis was prevented by optimizing the linker length between the REG–nanopore and α-subunit and by introducing a polyhistidine at the N-terminus of the REG–nanopore. The latter was introduced to shield the linker between subunits from cellular proteases (Supplementary Fig. 8d). A co-assembled proteasome–nanopore (mutant 8; Supplementary Figs. 8 and 9) was then purified in two steps by affinity chromatography (Supplementary Methods and Fig. 4b). SDS-PAGE, native PAGE, TEM and liquid chromatography with tandem mass spectrometry confirmed the successful assembly of the multiprotein complex (Fig. 4d,e, and Supplementary Figs. 5 and 10–12). Activity assays revealed that the proteasome–nanopore was active, with the proteolytic activity increasing with temperature and decreasing with salt concentration (Supplementary Fig. 13). The transmembrane proteasome inserted efficiently into lipid bilayers, whereas the spontaneous release from the lipid bilayer was not observed (Supplementary Fig. 4b). The proteasome–nanopores

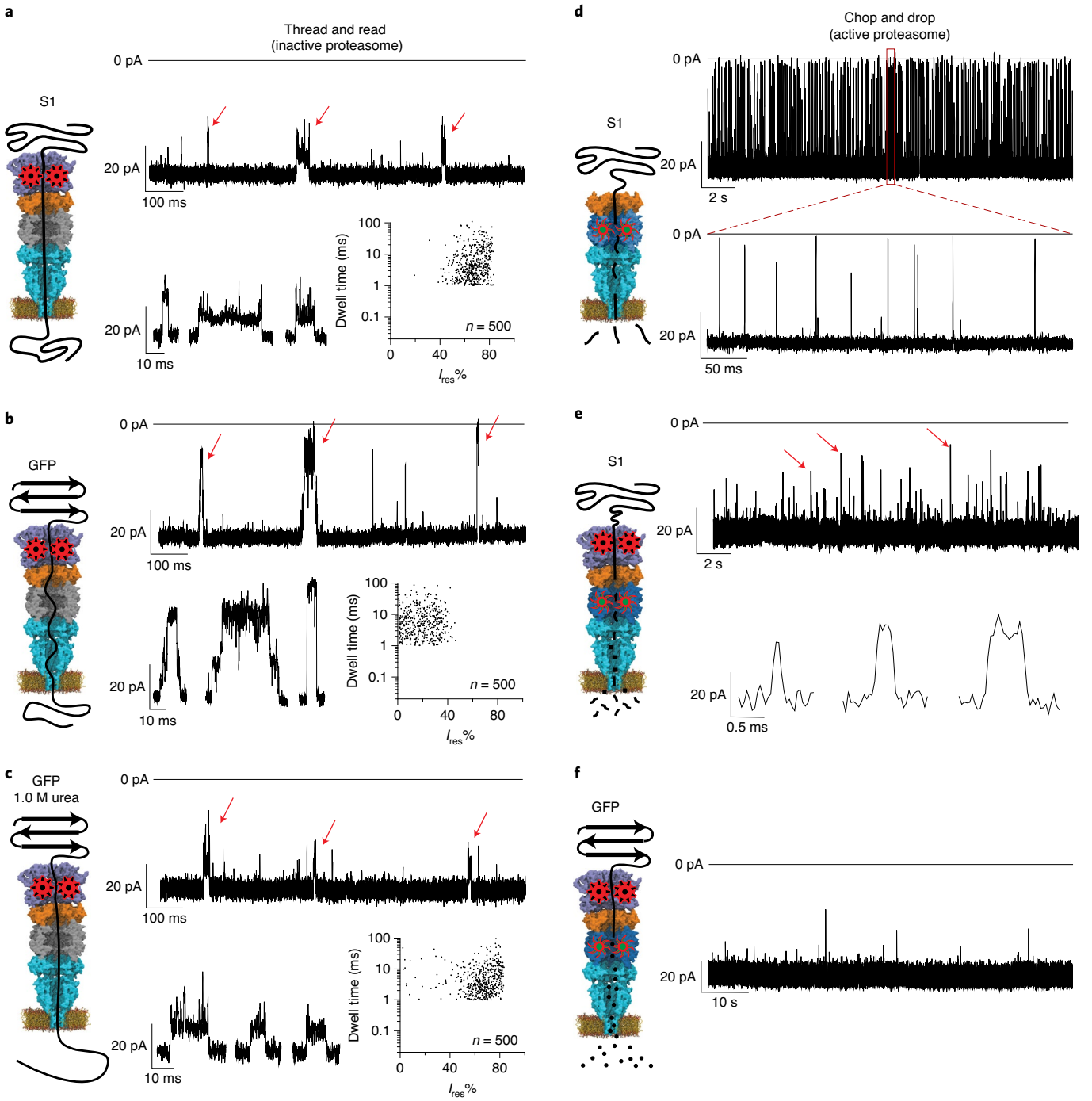

Fig. 5 | Controlled translocation through the proteasome–nanopore. a–c, Thread and read. Typical current traces and relative scatter plots showing the average I_{res}% versus dwell time provoked by the translocation of S1 (**a**, 20.0 μM S1 and 20.0 μM VATΔN; 23 independent nanopore experiments), GFP (**b**, 5.0 μM GFP and 5.0 μM VATΔN; 42 independent experiments) and GFP in 1 M urea (**c**, 5.0 μM GFP in 1 M urea and 5.0 μM VATΔN; 13 independent experiments) through an inactive proteasome–nanopore mediated by VATΔN in the presence of 2.0 mM ATP. Red arrows indicate the expanded ionic current blockades. The proteasome–nanopore and substrates were added to the *cis* side. **d–f**, Chop and drop. Typical current traces provoked by the transport of oligopeptides across an activated proteasome. **d**, Unassisted S1 translocation (>50 independent experiments). **e**, VATΔN- and ATP-assisted S1 transport induce fragmentation into small peptides, whereby fast transport is seldom observed (23 independent experiments). **f**, VATΔN-assisted GFP-ssrA proteolytic cleavages produce peptides that are too short to be detected by the nanopore (15 independent experiments). Data were collected at 40 °C and −30 mV in 1 M NaCl, 15 mM Tris, pH 7.5, using a 10 kHz low-pass Bessel filter with a 50 kHz sampling rate. The traces were then filtered digitally with a Gaussian low-pass filter with a 5 kHz cut-off.

showed low-noise current recordings at negative applied potentials (Fig. 4c); however, the proteasome–nanopore often gated at applied potentials higher than +20 mV (Supplementary Fig. 14). The different electrical properties allowed us to distinguish REG-nanopores from proteasome–nanopores, and allowed establishing that the subunits of the proteasome–nanopores did not

disassembled during the electrical recordings (Supplementary Fig. 15). The *I*–*V* curve of the proteasome–nanopore was similar to that of the REG–nanopore and to that of a proteasome–nanopore with a closed gate[29] (the latter maintains the N-terminals region of the α subunits atop of the REG–nanopore, which keeps the entry of the nanopore closed, Supplementary Fig. 16a). Similarly, the ion selectivity (Supplementary Fig. 16b) and the electrical noise of the proteasome–nanopore were also similar to that of the REG–nanopore (Supplementary Fig. 16c–e). These lines of evidence indicate that the transmembrane region of the proteasome–nanopore was unchanged compared with the REG–nanopore, and that the proteasome above the nanopore does not influence the ionic signal (see the Supplementary Information for further discussion).

Real-time protein processing. The activity of the transmembrane proteasome was tested using substrates containing a C-terminal ssrA tag, which mediates the interaction with valosin-containing protein-like ATPase of *T. acidophilum* (VAT)[30]. The latter is a processive hand-over-hand unfoldase that pulls on two extended residues of substrates through the proteasome chamber[31]. Here we used VATΔN[32], in which the first 183 amino acids of the N-terminal domain corresponding to a regulatory domain were deleted (Supplementary Fig. 17). VATΔN displays higher unfolding activity than wild-type (WT) VAT. We tested two substrates. The first, named S1 (123 amino acid residues), was designed to be unstructured. It contained an ssrA tag followed by four stretches of 15 serine residues, each flanked by ten arginine residues and three hydrophobic residues (FYW, Supplementary Fig. 18). The polyarginine residues were introduced to induce the electrophoretic transport across the nanopore, while the hydrophobic residues are ideal targets for the proteolytic activity of the proteasome[33]. The ssrA tag was introduced to allow VATΔN recognition[32]. Superfolder green fluorescent protein[34], which was modified by adding ten arginines and a ssrA tag at the C-terminus (here and throughout named simply GFP, Supplementary Fig. 18), was also tested. GFP was selected due to its high stability towards temperature denaturation (melting temperature 78 °C; ref. [35]) and chemotropic agents (unfolding at more than 4 M guanidine hydrochloride; ref. [36]), hence providing a good model system to test the limit of the proteasome–nanopore to unfold proteins. The activity of VATΔN was optimized using bulk assays (Supplementary Fig. 19). Hereafter, experiments were performed at 40 °C in 1 M NaCl, 15 mM Tris-HCl, pH 7.5, 20 mM $MgCl_2$ solutions. Tests were performed using either proteolytic active or inactive proteasome–nanopores. In the latter, the amino-terminal threonine 1 in the active site was replaced with alanine[15,37].

Thread and read. Two approaches to study single proteins become possible by using the proteasome–nanopore fabricated in this work. In the first, named thread and read, proteins are unfolded by VATΔN and thread across inactivated proteasome. The linearized polypeptide then translocates across the nanopore by the action of the electroosmotic flow. We tested this approach using S1 and GFP at 40 °C and −30 mV in 1 M NaCl, 15 mM Tris, pH 7.5. The addition of folded GFP to the *cis* side of a proteasome–nanopore induced no blockades. By contrast, the addition of unfolded and polycharged S1 induced many blockades that showed a residual current (I_{res}, defined as the percent ratio between the blocked nanopore current the open nanopore current) of 7.3 ± 0.1% (Supplementary Figs. 20b and 21b). The blockades were either short (with a dwell time of 0.30 ± 0.01 ms) or second-long (Supplementary Figs. 20b and 21b, and Supplementary Table 1). The shorter blockades probably reflect the translocation of S1 across the proteasome–nanopore and the long blockades reflect the occlusion of the proteasome chamber by the substrate. The reduced dwell time of S1 with increasing voltage (Supplementary Fig. 21) indicates that S1 translocate across the nanopore[38]. When an equal concentration of VATΔN and substrate protein in the presence of 2.0 mM ATP were added to the solution, S1 blockades became longer (6.64 ± 0.21 ms) and the I_{res}% increased by about tenfold (70.2 ± 1.0; Fig. 5a, and Supplementary Figs. 20 and 22), probably reflecting the VATΔN-assisted and stretched translocation of S1 across the nanopore. GFP blockades were also observed in the presence of VATΔN and ATP (Fig. 5b, and Supplementary Figs. 23 and 24), indicating that the unfoldase linearized and fed the substrate protein through the nanopore. GFP blockades were not observed in the absence of either VATΔN or ATP, or when PAN[39] unfoldase or WT-VAT (WT-VAT contains an N-terminal domain that inhibits its unfolding activity[32]) were used instead of VATΔN (Supplementary Fig. 25). When the ATP concentration was increased to 6.0 mM the average dwell time of GFP blockades decreased to 2.4 ± 1.7 ms (Supplementary Fig. 26), suggesting that VATΔN is capable of feeding the polypeptide through the nanopore at a speed that can be tuned by the concentration of ATP. Contrary to S1 blockades, VATΔN-assisted GFP blockades showed I_{res}% close to zero, suggesting the formation of secondary structures of the substrate protein inside the proteasomal chamber after VATΔN-unfolding and before translocating across the nanopore. In the presence of 1 M urea, GFP current blockades became similar to the blockades induced by unstructured S1 (with a dwell time of 7.8 ± 1.7 ms and an I_{res}% of 70.3 ± 0.9; Fig. 5a,c, and Supplementary Figs. 22 and 27). Urea probably prevented the partial refolding of the substrate allowing a stretched translocation across the nanopore after GFP was unfolded by VATΔN at the top of proteasome–nanopore. Although a stretched translocation across the nanopore is an important achievemnt, the electrical signal of individual events was relatively heterogeneous (Fig. 5a–c and Supplementary Figs. 22, 24, 26 and 27) and the identification of amino acids was not attainable. The latter might become possible by using a nanopore with subnanometre diameter, such as heptameric FraC[3], possibly coupled with a more uniform electroosmotic transport across the nanopore. Nonetheless, an important finding was that the unfolding of the protein above the nanopore did not affect the ionic signal (see the Supplementary Information for a more detailed discussion), indicating that the ionic signal can be entirely used for polypeptide identification.

Chop and drop. The enclosed architecture of the VATΔN-proteasome–nanopore allows a fundamentally new approach in single-molecule nanopore protein analysis, in which the proteasome cleaves an unfolded protein and the resulting peptides are recognized as they translocate the nanopore. We recently showed that the ionic signal from peptide blockades to a FraC nanopore relate directly to the volume of the peptide[3,4]. Hence, a proteasome–nanopore might be used as the equivalent of protein fingerprinting by mass spectrometry, but at the single-molecule level. We tested this approach using S1 and GFP. When an active proteasome–nanopore was used, the second-long blockades observed during unassisted S1 translocation disappeared whereas the short blockades became faster (0.20 ± 0.01 ms; Fig. 5d and Supplementary Fig. 28a). These results therefore suggest that the proteasome processes the substrates as they translocate across the nanopore. When VATΔN and ATP were added in solution, more spaced and shorter blockades were observed (Fig. 5e and Supplementary Fig. 28b), indicating that the reduced speed of polypeptide threading across the proteasomal chamber allowed the degradation of S1 into smaller peptides that are quickly transported across the nanopore. Accordingly, when GFP was tested under the same conditions fewer blockades were observed. The size limit of peptide detection of the REG–nanopore is approximately ten amino acids (Fig. 3h–j and Supplementary Fig. 7e), whereas the proteasome has been shown to produce peptide fragments between around six and ten amino acids depending on the protein substrate[40]. In turn, this suggests that the slower unfolding of GFP compared with the unstructured S1 allowed for a

more efficient proteolysis of the substrate into yet smaller peptides (Fig. 5), which are transported across the nanopore too quickly to be observed. Although further improvements will be required for allowing single-molecule fingerprinting (for example, changing the nanopore size or tuning the proteolytic pattern of the proteasome), this work present the first important demonstration that small molecule products of an enzymatic reaction can be addressed by a nanopore.

In conclusion, this work describes a strategy to build nanopores with advanced functionalities. Soluble proteins with a toroidal shape can be inserted into a lipid membrane by replacing a loop on the protein surface with the transmembrane region of a β-barrel pore flanked by a short hydrophilic linker. The artificial nanopores inserted efficiently into lipid bilayers and showed a well-defined β-barrel structure. Bespoke optimizations of the length and composition of the hydrophilic linker allowed to engineer a nanopore that displayed low current noise and remained constantly open under an applied potential. Using this approach, we fabricated from the bottom up a 42-protein component nanopore sensor that is capable of processing folded proteins. This multiprotein molecular machine opens the door to two new potential approaches in single-molecule protein characterization, in which individual proteins are addressed by a nanopore either as intact linearized polypeptides or as a pattern of fragmented peptides.

Online content

Any methods, additional references, Nature Research reporting summaries, source data, extended data, supplementary information, acknowledgements, peer review information; details of author contributions and competing interests; and statements of data and code availability are available at https://doi.org/10.1038/s41557-021-00824-w.

Received: 19 January 2021; Accepted: 22 September 2021;
Published online: 18 November 2021

References

1. Bayley, H. Nanopore sequencing: from imagination to reality. *Clin. Chem.* **61**, 25–31 (2014).
2. Kang, X. F., Cheley, S., Guan, X. & Bayley, H. Stochastic detection of enantiomers. *J. Am. Chem. Soc.* **128**, 10684–10685 (2006).
3. Huang, G., Voet, A. & Maglia, G. FraC nanopores with adjustable diameter identify the mass of opposite-charge peptides with 44 dalton resolution. *Nat. Commun.* **10**, 1–10 (2019).
4. Huang, G., Willems, K., Soskine, M., Wloka, C. & Maglia, G. Electro-osmotic capture and ionic discrimination of peptide and protein biomarkers with FraC nanopores. *Nat. Commun.* **8**, 935 (2017).
5. Restrepo-Pérez, L., Wong, C. H., Maglia, G., Dekker, C. & Joo, C. Label-free detection of post-translational modifications with a nanopore. *Nano Lett.* **19**, 7957–7964 (2019).
6. Ouldali, H. et al. Electrical recognition of the twenty proteinogenic amino acids using an aerolysin nanopore. *Nat. Biotechnol.* **38**, 176–181 (2020).
7. Hu, Z.-L., Huo, M.-Z., Ying, Y.-L. & Long, Y.-T. Biological nanopore approach for single-molecule protein sequencing. *Angew. Chemie* **60**, 14738–14749 (2020).
8. Nivala, J., Mulroney, L., Li, G., Schreiber, J. & Akeson, M. Discrimination among protein variants using an unfoldase-coupled nanopore. *ACS Nano* **8**, 12365–12375 (2014).
9. Nivala, J., Marks, D. B. & Akeson, M. Unfoldase-mediated protein translocation through an α-hemolysin nanopore. *Nat. Biotechnol.* **31**, 247–250 (2013).
10. Xu, C. et al. Computational design of transmembrane pores. *Nature* **585**, 129–134 (2020).
11. Joh, N. H. et al. De novo design of a transmembrane Zn^{2+}-transporting four-helix bundle. *Science* **346**, 1520–1520 (2014).
12. Lu, P. et al. Accurate computational design of multipass transmembrane proteins. *Science* **359**, 1042–1046 (2018).
13. Scott, A. et al. Constructing ion channels from water-soluble α-helical barrels. *Nat. Chem.* **13**, 643–650 (2021).
14. Spruijt, E., Tusk, S. E. & Bayley, H. DNA scaffolds support stable and uniform peptide nanopores. *Nat. Nanotechnol.* **13**, 739–745 (2018).
15. Seemüller, E. et al. Proteasome from *Thermoplasma acidophilum*: a threonine protease. *Science* **268**, 579–582 (1995).
16. Löwe, J. et al. Crystal structure of the 20S proteasome from the archaeon *T. acidophilum* at 3.4 Å resolution. *Science* **268**, 533–539 (1995).
17. Sugiyama, M. et al. Spatial arrangement and functional role of α subunits of proteasome activator PA28 in hetero-oligomeric form. *Biochem. Biophys. Res. Commun.* **432**, 141–145 (2013).
18. Förster, A., Masters, E. I., Whitby, F. G., Robinson, H. & Hill, C. P. The 1.9 Å structure of a proteasome-11S activator complex and implications for proteasome-PAN/PA700 interactions. *Mol. Cell* **18**, 589–599 (2005).
19. Jiang, J., Pentelute, B. L., Collier, R. J. & Hong Zhou, Z. Atomic structure of anthrax protective antigen pore elucidates toxin translocation. *Nature* **521**, 545–549 (2015).
20. Cheley, S., Braha, O., Lu, X., Conlan, S. & Bayley, H. A functional protein pore with a "retro" transmembrane domain. *Protein Sci.* **8**, 1257–1267 (1999).
21. Gu, L. Q. et al. Reversal of charge selectivity in transmembrane protein pores by using noncovalent molecular adapters. *Proc. Natl Acad. Sci. USA* **97**, 3959–3964 (2000).
22. Maglia, G., Restrepo, M. R., Mikhailova, E. & Bayley, H. Enhanced translocation of single DNA molecules through α-hemolysin nanopores by manipulation of internal charge. *Proc. Natl Acad. Sci. USA* **105**, 19720–19725 (2008).
23. Chen, B. et al. Engagement of arginine finger to ATP triggers large conformational changes in NtrC1 AAA+ ATPase for remodeling bacterial RNA polymerase. *Structure* **18**, 1420–1430 (2010).
24. Gu, L. Q., Braha, O., Conlan, S., Cheley, S. & Bayley, H. Stochastic sensing of organic analytes by a pore-forming protein containing a molecular adapter. *Nature* **398**, 686–690 (1999).
25. Yannakopoulou, K. et al. Symmetry requirements for effective blocking of pore-forming toxins: comparative study with α-, β-, and γ-cyclodextrin derivatives. *Antimicrob. Agents Chemother.* **55**, 3594–3597 (2011).
26. Förster, A. & Hill, C. P. Proteasome activators. *Protein Degrad.* **2**, 89–110 (2007).
27. Huber, E. M. & Groll, M. The mammalian proteasome activator PA28 forms an asymmetric α4β3 complex. *Structure* **25**, 1473–1480.e3 (2017).
28. Kuehn, L. & Dahlmann, B. Proteasome activator PA28 and its interaction with 20S proteasomes. *Arch. Biochem. Biophys.* **329**, 87–96 (1996).
29. Benaroudj, N., Zwickl, P., Seemüller, E., Baumeister, W. & Goldberg, A. L. ATP hydrolysis by the proteasome regulatory complex PAN serves multiple functions in protein degradation. *Mol. Cell* **11**, 69–78 (2003).
30. Huang, R. et al. Unfolding the mechanism of the AAA+ unfoldase VAT by a combined cryo-EM, solution NMR study. *Proc. Natl Acad. Sci. USA* **113**, E4090–W4199 (2016).
31. Ripstein, Z. A., Huang, R., Augustyniak, R., Kay, L. E. & Rubinstein, J. L. Structure of a AAA+ unfoldase in the process of unfolding substrate. *eLife* **6**, 1–14 (2017).
32. Gerega, A. et al. VAT, the Thermoplasma homolog of mammalian p97/VCP, is an N domain-regulated protein unfoldase. *J. Biol. Chem.* **280**, 42856–42862 (2005).
33. Akopian, T. N., Kisselev, A. F. & Goldberg, A. L. Processive degradation of proteins and other catalytic properties of the proteasome from Thermoplasma acidophilum. *J. Biol. Chem.* **272**, 1791–1798 (1997).
34. Pédelacq, J. D., Cabantous, S., Tran, T., Terwilliger, T. C. & Waldo, G. S. Engineering and characterization of a superfolder green fluorescent protein. *Nat. Biotechnol.* **24**, 79–88 (2006).
35. Ward, W. W., Prentice, H. J., Roth, A. F., Cody, C. W. & Reeves, S. C. Spectral perturbations of the aequorea green-fluorescent protein. *Photochem. Photobiol.* **35**, 803–808 (1982).
36. Hsu, S.-T. D., Blaser, G. & Jackson, S. E. The folding, stability and conformational dynamics of β-barrel fluorescent proteins. *Chem. Soc. Rev.* **38**, 2951–2965 (2009).
37. Kisselev, A. F., Songyang, Z. & Goldberg, A. L. Why does threonine, and not serine, function as the active site nucleophile in proteasomes? *J. Biol. Chem.* **275**, 14831–14837 (2000).
38. Biesemans, A., Soskine, M. & Maglia, G. A protein rotaxane controls the translocation of proteins across a ClyA nanopore. *Nano Lett.* **15**, 6076–6081 (2015).
39. Majumder, P. et al. Cryo-EM structures of the archaeal PAN-proteasome reveal an around-the-ring ATPase cycle. *Proc. Natl Acad. Sci. USA* **116**, 534–539 (2019).
40. Kisselev, A. F., Akopian, T. N. & Goldberg, A. L. Range of sizes of peptide products generated during degradation of different proteins by archaeal proteasomes. *J. Biol. Chem.* **273**, 1982–1989 (1998).

Methods

A detailed description of the methodology can be found in the Supplementary Information. A short description is given here.

General materials. Oligonucleotides and gBlock gene fragments were obtained from Integrated DNA Technologies. All enzymes were purchased from Fisher Scientific. All peptides and chemicals were obtained from Sigma-Aldrich. 1,2-Diphytanoyl-sn-glycero-3-phosphocholine was purchased from Avanti Polar Lipids.

Plasmid construction for proteins. All gBlock gene fragments were ordered for synthesis by Integrated DNA Technologies. Plasmid and gene were ligated together using T4 ligase (Fermentas). The identity of the clones was confirmed by sequencing at Macrogen.

Data recordings and analysis. Current recordings were performed in a planar bilayer set-up as described previously[41]. Electronic signals were recorded by using an Axopatch 200B (Axon Instruments) with digitization performed with a Digidata 1440 (Axon Instruments). Clampex 10.7 software and Clampfit 10.7 software (Molecular Devices) were used for electronic signal recording and subsequent data analysis, respectively. Events were collected using the single-channel search feature in Clampfit.

Data availability

All relevant data are included in the article and its Supplementary Information. Statistical source data, unmodified gels, and molecular dynamics simulations results are provided in Source data. Data is also available from the authors upon reasonable request. Source data are provided with this paper.

References

41. Maglia, G., Heron, A. J. J., Stoddart, D., Japrung, D. & Bayley, H. Analysis of single nucleic acid molecules with protein nanopores. *Methods Enzym.* **475**, 591–623 (2010).

Acknowledgements

This work is financially supported by ERC consolidator grant (no. 726151).

Author contributions

S.Z. and G.M. designed the experiments. G.M. supervised the project. S.Z. performed the experiments and data analysis. B.M.H.B., P.C.T.d.S. and S.-J.M. conducted the simulation work. G.M. and S.Z. wrote the paper. All authors discussed the results, and commented on the manuscript.

Competing interests

G.M. is a founder, director and shareholder of Portal Biotech Limited, a company engaged in the development of nanopore technologies. This work was not supported by Portal Biotech Limited.

Additional information

Supplementary information The online version contains supplementary material available at https://doi.org/10.1038/s41557-021-00824-w.

Correspondence and requests for materials should be addressed to Giovanni Maglia.

Peer review information *Nature Chemistry* thanks Ulrich Keyser, Yi-Lun Ying and the other, anonymous, reviewer(s) for their contribution to the peer review of this work.

Reprints and permissions information is available at www.nature.com/reprints.